

SHADOW OF REGULAR BLACK HOLE IN SCALAR-TENSOR-VECTOR GRAVITY THEORY

Subhadip Sau^{*1,2}  and John W. Moffat^{†3,4}

¹*Department of Physics, Jhargram Raj College, Jhargram, West Bengal-721507*

²*School of Physical Sciences, Indian Association for the Cultivation of Science,
2A & 2B Raja S. C. Mullick Road, Kolkata-700032, India*

³*Perimeter Institute for Theoretical Physics, Waterloo, Ontario N2L 2Y5, Canada*

⁴*Department of Physics and Astronomy, University of Waterloo, Waterloo, Ontario N2L 3G1, Canada*

September 9, 2024

Abstract

We investigate the shadow cast by a regular black hole in scalar-tensor-vector modified gravity theory. This black hole differs from a Schwarzschild-Kerr black hole by the dimensionless parameter β . The size of the shadow depends on this parameter. Increasing the value of the parameter β shrinks the shadow. A critical value of the parameter β is found to be $\beta_{\text{crit}} = 0.40263$. The shadow for the horizonless dark compact object has been analysed for the static, spherically symmetric case and compared with M87* and Sgr A* data. Shadow observables have been determined in the context of the regular black hole and used for obtaining the energy emission rate. The peak of the energy emission rate shifts to lower frequency for the increasing value of the parameter β .

*subhadipsau2@gmail.com

†jwmoffat@perimeterinstitute.ca

Contents

1	Introduction	2
2	STVG action and field Equations	3
3	Static regular MOG compact object	5
4	Regular MOG static spherically symmetric spacetime	7
4.1	Motion of photons in MOG spherically symmetric spacetime	8
4.2	Parameter estimation using M87* and Sgr A* data	9
5	Regular MOG rotating compact object	14
6	Analysis of the black hole shadow	16
6.1	Null geodesics	16
6.2	Celestial coordinates and shadow structure	19
6.3	Observables	19
7	Energy emission rate for the rotating regular MOG black hole	22
8	Conclusions	25

1 Introduction

One of the most remarkable predictions of the general theory of relativity is the occurrence of black holes. The recent observations by the Event Horizon Telescope (EHT) collaboration [1–7] and the detection of gravitational wave signals by the Laser-Interferometer Gravitational Wave-Observatory (LIGO) and Virgo [8–10], corroborate the existence of these celestial objects. Despite its success, the theory of general relativity is not flawless. The two major drawbacks of this theory are the presence of singularities [11, 12] in the theory and the lack of observational data verifying the existence of the dark sector [13]. The research community is divided into two groups regarding this issue [14–19]. Either dark matter exists or alternatively Einstein’s gravitational theory has to be modified. Despite numerous attempts to find the existence of the dark sector, in particular, the dark matter, all experimental attempts to detect dark matter have until now failed [20, 21]. This motivates us to explore the nature of black holes in a theory where these above mentioned ambiguities are removed. One of the successful approaches towards this goal has been developed by one of the authors [22]. The theory is popularly known in the literature as the scalar-tensor-vector gravity (STVG) theory and MODified gravity (MOG). The solar system observations [23], cosmological observations [24], galaxy rotation curves [25–27] and the dynamics of galaxy clusters [28, 29] have all been satisfactorily explained by the MOG. It has also been successful in describing structure growth, the matter power spectrum, and cosmic microwave background (CMB) acoustical and angular power spectrum data [30–33]. Observational signatures and constrains of the black holes and other compact objects as appearing in MOG theory have been discussed in the literature [34–36]. To

distinguish the MOG theory from general relativity, EHT observational data have been used to study the shadow cast by the supermassive MOG black holes Sgr A* and M87* [37].

As a result of lensing phenomena [38–41], the black hole scatters the higher angular momentum photons from the source, sending them to the distant observer, while the photons with less angular momentum fall into the black hole and create a shadow zone and a possible light ring. The black hole shadow, which develops next to the event horizon, gives us a general notion of the fundamental geometrical structure of horizons [42]. A review of these developments can be found in [43]. Sagittarius A*, the supermassive black hole at the heart of our galaxy, and M87* at the galactic centre of M87 have both been confirmed by the EHT astronomical observations [1–7]. A two-dimensional dark disc encircled by bright rings is the black hole’s observable appearance. The light rings are photon orbits, while the dark area represents the black hole shadow. The accreted matter around the black hole has an impact on how the shadow is shaped. Since the black hole’s shadow carries the geometry of the surrounding region in its shape and size, it is considered a helpful tool for determining the black hole’s spin and other deformation characteristics and parameters [44–47]. This in turn can help to distinguish and test general relativity and other alternative theories [48–65]. The black hole candidates display a significant rotation. Our main goal will be to explore the rotating black holes in MOG/STVG theory. To evade the problem of a singularity, we will focus our study on regular solutions in the STVG/MOG theory of gravity. One of the crucial methods for obtaining information about a black hole is the study of its shadow [66–71]. Earlier attempts have been made to analyse the shadows of regular black holes [54,72–78]. Many of these regular black holes arise from gravity coupled to non-linear electrodynamics. However, the electrical charge of black holes is expected to have negligible effect on the geometry of spacetime [79]. In STVG/MOG theory, the regular black hole solutions are obtained from a purely gravitational theory and can be potential candidates for astrophysical black holes.

The paper is organized as follows: In [Section 2](#) a brief introduction to the STVG/MOG gravitational action and field equations is presented. The static regular MOG compact object is discussed in [Section 3](#). In [Section 4](#), we investigate the regular MOG spherically symmetric solution and analytically derive the critical value of the parameter β . We also derive the parameter dependence of the black hole horizon, photon sphere and shadow. [Section 5](#) is dedicated to a study of the regular MOG rotating solution. In [Section 6](#), we have determined the shape and size of the black hole shadow for the regular MOG rotating solution along with the observables associated with it. Finally we have calculated the energy emission rate for the concerned black hole with the help of associated observables in [Section 7](#).

Throughout the paper, we will use mostly the positive metric convention assuming the velocity of light to be unity ($c = 1$).

2 STVG action and field Equations

The action for MOG/ STVG theory is

$$S = S_{\text{GR}} + S_{\phi} + S_S + S_M \quad (1)$$

where

$$S_{\text{GR}} = \frac{1}{16\pi} \int d^4x \sqrt{-g} \frac{1}{G} R \quad (2)$$

$$S_\phi = - \int d^4x \sqrt{-g} \left(\frac{1}{4} B^{\mu\nu} B_{\mu\nu} - \frac{1}{2} \mu^2 \phi^\mu \phi_\mu - J^\mu \phi_\mu \right) \quad (3)$$

$$S_S = \int d^4x \sqrt{-g} \frac{1}{G^3} \left(\frac{1}{2} g^{\mu\nu} \nabla_\mu G \nabla_\nu G - V(G) - JG \right) + \int d^4x \sqrt{-g} \frac{1}{\mu^2 G} \left(\frac{1}{2} g^{\mu\nu} \nabla_\mu \mu \nabla_\nu \mu - V(\mu) \right) \quad (4)$$

Here $g_{\mu\nu}$ is the spacetime metric, g is the determinant of the metric, R is the Ricci scalar, ϕ^μ is a proca-type massive vector field such that $B_{\mu\nu} = \partial_\mu \phi_\nu - \partial_\nu \phi_\mu$, $G(x)$ and $\mu(x)$ are scalar fields and $V(G)$ and $V(\mu)$ are the corresponding potentials. S_M is the matter action. The energy-momentum tensor for the gravitational source can be written as

$$T_{\mu\nu} = T_{\mu\nu}^M + T_{\mu\nu}^\phi + T_{\mu\nu}^S \quad (5)$$

where

$$T_{\mu\nu}^M = - \frac{2}{\sqrt{-g}} \frac{\partial S_M}{\delta g^{\mu\nu}} \quad (6a)$$

$$T_{\mu\nu}^\phi = - \frac{2}{\sqrt{-g}} \frac{\partial S_\phi}{\delta g^{\mu\nu}} \quad (6b)$$

$$T_{\mu\nu}^S = - \frac{2}{\sqrt{-g}} \frac{\partial S_S}{\delta g^{\mu\nu}} \quad (6c)$$

Here, $T_{\mu\nu}^M$ is the ordinary matter energy-momentum tensor, $T_{\mu\nu}^\phi$ is the energy-momentum tensor for the field ϕ^μ and the scalar contribution to the energy-momentum tensor is denoted by $T_{\mu\nu}^S$. Moreover, J^μ and J are the vector and scalar field currents, respectively.

The Schwarzschild-MOG and Kerr-MOG black hole solutions can be found with the following assumptions:

- It is assumed that the matter energy-momentum tensor $T_{\mu\nu}^M$ and the vector and scalar field currents J^μ and J are zero.
- Since the effects of the vector field ϕ_μ mass μ becomes prominent at kiloparsec distances from the source, the mass of the vector field is disregarded when solving the field equations for compact objects like black holes.
- The constant G depends on the parameter $\beta = \alpha/(1 + \alpha)$ by $G = G_N(1 + \alpha) = \frac{G_N}{1 - \beta}$. Here, G_N is Newton's gravitational constant and we assume that $\partial_\mu G \approx 0$. The range of the dimensionless parameter β is $0 \leq \beta \leq 1$.

The action in Eq. (1) assumes the following form:

$$S = \frac{1}{16\pi G} \int d^4x \sqrt{-g} \left(R - \frac{1}{4} B^{\mu\nu} B_{\mu\nu} \right) \quad (7)$$

Varying this action with respect to $g_{\mu\nu}$, we get the following field equations:

$$G_{\mu\nu} = 8\pi G T_{\mu\nu}^\phi \quad (8)$$

Here $G_{\mu\nu}$ is the Einstein tensor $R_{\mu\nu} - \frac{1}{2}g_{\mu\nu}R$. The energy-momentum tensor associated with vector field ϕ_μ is given by

$$T_{\mu\nu}^\phi = \frac{1}{4\pi} \left(B_{\mu}{}^\rho B_{\nu\rho} - \frac{1}{4}g_{\mu\nu}B^{\alpha\beta}B_{\alpha\beta} \right) \quad (9)$$

To obtain the dynamical equation for the vector field, we need to vary the action in Eq. (7) with respect to the vector field ϕ_μ . Such a variation leads to the following dynamical equation:

$$\nabla_\nu B^{\mu\nu} = \frac{1}{\sqrt{-g}}\partial_\nu(\sqrt{-g}B^{\mu\nu}) = 0 \quad (10)$$

One should note here that the gravitational charge Q_g associated with the MOG vector field is proportional to the mass of the gravitational source as [80]

$$Q_g = \sqrt{\alpha G_N} M = \sqrt{\beta(1-\beta)G_N} M_\beta \quad (11)$$

where $M_\beta = (1+\alpha)M$. The gravitational charge Q_g results in the modified Newtonian acceleration for weak gravitational fields and slow particle motion:

$$a(r) = -\frac{G_N M}{r^2} [1 + \alpha - \alpha \exp(-\mu r)(1 + \mu r)] \quad (12)$$

For small scale objects and weak gravitational fields $\mu r \ll 1$ and the parameter α cancels, reducing the acceleration to Newtonian gravity. With parameter-post-Newtonian corrections this guarantees that MOG is consistent with accurate solar system experiments.

3 Static regular MOG compact object

The gravitational action for the matter-free MOG theory using non-linear field equations for the gravitational spin 1 vector field ϕ_μ is given by [81]

$$S_{\text{MOG}} = \frac{1}{16\pi G} \int d^4x \sqrt{-g} [R - L(B)] \quad (13)$$

where R is the Ricci scalar, $L(B)$ describes the non-linear contribution of $B_{\mu\nu} = \partial_\mu\phi_\nu - \partial_\nu\phi_\mu$ with $B = \frac{1}{4}B_{\mu\nu}B^{\mu\nu}$. The associated field equations are

$$G_{\mu\nu} = 8\pi G T_{\mu\nu}^\phi \quad (14a)$$

$$\nabla_\nu \left(\frac{\partial L}{\partial B} B^{\mu\nu} \right) = 0 \quad (14b)$$

$$\nabla_\mu (*B^{\mu\nu}) = 0 \quad (14c)$$

where $*B^{\mu\nu} = \epsilon^{\mu\nu\rho\sigma}B_{\rho\sigma}$ is the Hodge-dual of $B^{\mu\nu}$. The energy-momentum tensor associated with the theory is given by

$$T_{\mu\nu}^\phi = \frac{1}{4\pi} \left[\frac{\partial L}{\partial B} g^{\rho\sigma} B_{\mu\rho} B_{\nu\sigma} - g_{\mu\nu} L(B) \right] \quad (15)$$

In this theory, the gravitational constant is enhanced by $G = G_N(1 + \alpha)$. The gravitational source charge associated with the vector field ϕ_μ is given by

$$Q_g = \sqrt{\alpha G_N M} \quad (16)$$

where M is the mass parameter of the theory. The gravi-electric field is given by

$$E_{\text{grav}}(r) = B_{01}(r) = -B_{10}(r) \quad (17)$$

The energy-momentum tensor components are given by

$$T_0^{\phi 0} = T_1^{\phi 1} = -\frac{1}{4\pi} \left(E_{\text{grav}}^2 \frac{\partial L}{\partial B} + L(B) \right) \quad (18)$$

To describe the non-linear system in an alternative way, one can consider the function H obtained from the Legendre transformation. The function H is given by

$$H = 2B \frac{\partial L}{\partial B} - L(B) \quad (19)$$

We assume

$$P_{\mu\nu} = \frac{\partial L}{\partial B} B_{\mu\nu} \quad (20)$$

and

$$P = \frac{1}{4} P_{\mu\nu} P^{\mu\nu} = \left(\frac{\partial L}{\partial B} \right)^2 B \quad (21)$$

Now, H can be expressed as the function of P . For the regular spacetime metric solution the form of the function $H(P)$ is given by

$$H(P) = P \frac{\left(1 - 3\sqrt{-2\alpha(1+\alpha)M^2P} \right)}{\left(1 + \sqrt{-2\alpha(1+\alpha)M^2P} \right)^3} - \frac{3}{2\alpha(1+\alpha)M^2b} \left(\frac{\sqrt{-2\alpha(1+\alpha)M^2P}}{1 + \sqrt{-2\alpha(1+\alpha)M^2P}} \right) \quad (22)$$

where $b = \frac{\sqrt{\alpha}M}{2}$ and $P = -\frac{\alpha}{(1+\alpha)} \frac{M^2}{2r^4}$ and we have set the gravitational constant $G_N = 1$. The associated Lagrangian L is provided by

$$L(P) = P \frac{\left(1 - 8\sqrt{-2\alpha(1+\alpha)M^2P} - 6\alpha(1+\alpha)M^2P \right)}{\left(1 + \sqrt{-2\alpha(1+\alpha)M^2P} \right)^4} - \frac{3(-2\alpha(1+\alpha)M^2P)^{5/4} \left(3 - \sqrt{-2\alpha(1+\alpha)M^2P} \right)}{4\alpha(1+\alpha)M^2b \left(1 + \sqrt{-2\alpha(1+\alpha)M^2P} \right)^{7/2}} \quad (23)$$

4 Regular MOG static spherically symmetric spacetime

The MOG regular, static spherically symmetric solution can be written as [81, 82]

$$ds^2 = -f(r)dt^2 + \frac{1}{f(r)}dr^2 + r^2(d\theta^2 + \sin^2\theta d\phi^2) \quad (24)$$

with

$$f(r) = 1 - \frac{2(1+\alpha)Mr^2}{(r^2 + \alpha(1+\alpha)M^2)^{3/2}} + \frac{\alpha(1+\alpha)M^2r^2}{(r^2 + \alpha(1+\alpha)M^2)^2} \quad (25)$$

Here M is the mass parameter of the gravitating object. The associated gravi-electric field is given by

$$E_{\text{grav}}(r) = \sqrt{\alpha}Mr^4 \left[\frac{r^2 - 5\alpha(1+\alpha)M^2}{\{r^2 + \alpha(1+\alpha)M^2\}^4} + \frac{15}{2} \frac{(1+\alpha)M}{\{r^2 + \alpha(1+\alpha)M^2\}^{7/2}} \right] \quad (26)$$

For a convenient way of studying the theory, we introduce the alternative parameter β as

$$\beta = \frac{\alpha}{1+\alpha} \quad (27)$$

The ADM mass of the gravitating object is

$$M_{\text{ADM}} = (1+\alpha)M = \frac{M}{1-\beta} \equiv M_\beta \quad (28)$$

We can express the metric in Eq. (24) in terms of the ADM mass with

$$f(r) = 1 - \frac{2M_\beta r^2}{(r^2 + \beta M_\beta^2)^{3/2}} + \frac{\beta M_\beta^2 r^2}{(r^2 + \beta M_\beta^2)^2} \quad (29)$$

Here M_β is the ADM mass of the spacetime and β is the enhancement parameter. The gravitational source charge in terms of the ADM mass is given by

$$Q_g = \sqrt{\beta(1-\beta)G_N}M_\beta \quad (30)$$

The horizon of the spacetime depends on the zeros of the function $f(r)$ and that can be used to determine the critical value of the parameter β . Let us assume $\frac{r^2}{M_\beta^2} + \beta = x^2$, then zeros of $f(r)$ can be determined by the equation

$$ax^4 + bx^3 + cx^2 + dx + e = 0 \quad (31)$$

where, $a = 1, b = -2, c = \beta, d = 2\beta, e = -\beta^2$. The discriminant of the quartic equation is

$$\Delta = 256a^3e^3 - 192a^2bde^2 - 128a^2c^2e^2 + 144a^2cd^2e - 27a^2d^4$$

$$\begin{aligned}
& + 144ab^2ce^2 - 6ab^2d^2e - 80abc^2de + 18abcd^3 + 16ac^4e \\
& - 4ac^3d^2 - 27b^4e^2 + 18b^3cde - 4b^3d^3 - 4b^2c^3e + b^2c^2d^3 \\
& = -4\beta^2(27 + 4\beta[-16 + \beta\{20 + \beta(-28 + 25\beta)\}])
\end{aligned} \tag{32}$$

As the discriminant satisfies $\Delta \leq 0$, there will be two distinct real roots of the quartic equation. The critical value at which there will be only one horizon is given by the solution of the equation

$$10800\beta^3 - 12096\beta^2 + 20304\beta - 6912 = 0 \tag{33}$$

The solution of this equation is $\beta = 0.402186 = \beta_{\text{crit}}$. For $\beta < \beta_{\text{crit}}$ there will be a black hole with two horizons [80] and there will be no horizon for $\beta > \beta_{\text{crit}}$. This result is displayed in Fig. [1].

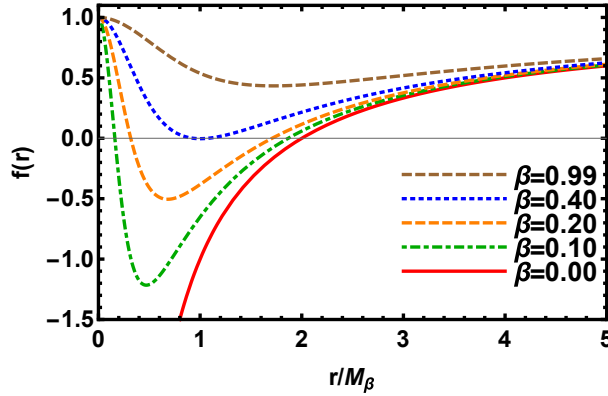


Figure 1: The zeros of the function $f(r)$ have been shown to confirm that either two horizons or no horizon are possible for the regular MOG spherically symmetric spacetime. For $\beta = 0$ the spacetime becomes Schwarzschild and has a singularity at $r = 0$. One horizon solution is possible for the critical value of the parameter $\beta_{\text{crit}} \approx 0.40263$. It is easy to check that there is no singularity for non-zero values of parameter β .

4.1 Motion of photons in MOG spherically symmetric spacetime

The Lagrangian for the photon motion is given by

$$\mathcal{L} = \frac{1}{2} \left[-f(r)\dot{t}^2 + \frac{1}{f(r)}\dot{r}^2 + r^2\dot{\theta}^2 + r^2\sin^2\theta\dot{\phi}^2 \right] \tag{34}$$

For a spherically symmetric spacetime, we can always choose without loss of generality $\theta = \pi/2$ and $\dot{\theta} = 0$. The equations for \dot{t} and $\dot{\phi}$ can be deduced using the symmetries of the MOG regular, static spherically symmetric spacetime. The associated equations are

$$f(r)\dot{t} = E \tag{35}$$

$$r^2\dot{\phi} = L \tag{36}$$

where E and L are, respectively, the energy and angular momentum of the photon. The radial equation can be written as

$$\dot{r}^2 + V(r) = E^2 \quad (37)$$

where, $V(r) = L^2 \frac{f(r)}{r^2}$. The structure of the potential helps to determine the presence of stable or/and unstable circular orbits. From Fig. [2], we conclude that for the whole parameter space, there exists a stable circular orbit and an unstable circular orbit. This special situation arises for $\beta_{\text{crit}} < \beta \lesssim 0.5$. However, with close inspection and from Fig. [3a] for $\beta < \beta_{\text{crit}}$, we only have unstable circular orbits.

As assumed earlier, $r^2/M_\beta^2 + \beta = x^2$ can be used to find the position of the photon sphere. The position of the photon sphere can be found by the real greatest solution of the following equation

$$x^4 - 3x^3 + 2\beta x^2 + 5\beta x - 3\beta^2 = 0 \quad (38)$$

For $\beta < \beta_{\text{crit}}$, there will be a photon sphere and a gradual increase in the enhancement parameter β causes the decrease of both the horizon and shadow radius. For the dark compact object with $\beta_{\text{crit}} < \beta \lesssim 0.5$, although there is no horizon, we still have a photon sphere. In spherically symmetric spacetimes, the shadow of the black hole is circular in structure. For the regular MOG black holes, the shadow has been shown with the variation in the parameter β in Fig. [3b]. In the figures, A and B are the celestial coordinates.

4.2 Parameter estimation using M87* and Sgr A* data

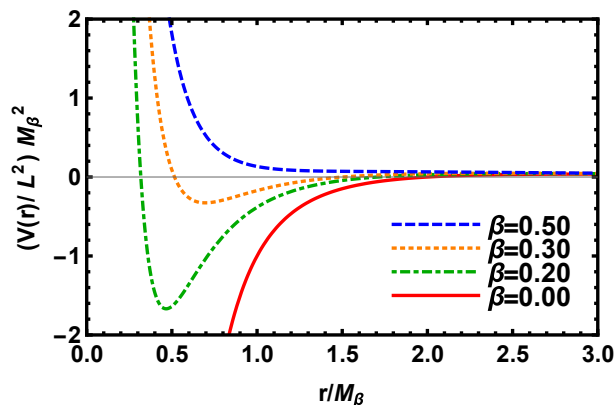
Although astrophysical black holes are rotating in nature, for a first-hand estimation of black hole parameters, one can use the shadow of the spherically symmetric black holes. As the shadow for spherically symmetric black holes does not depend on the inclination angle to obtain the initial estimation of the parameter β , we can work with the shadow of the regular MOG black hole solution. Apart from this, the observed shadows for M87* and Sgr A* are more or less circular in nature. This motivates us to find the observational signatures of the regular MOG black hole or compact objects in M87* and Sgr A* using EHT data.

We have calculated how the radius of the photon sphere and the shadow affected the parameter β in the previous section. We can determine the values of β based on the size of the angular diameter, which is defined as

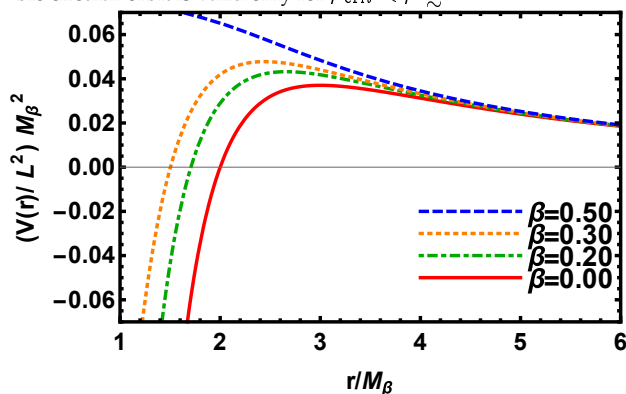
$$\tan \alpha \approx \alpha = \frac{r_{sh}}{D} \quad (39)$$

Where r_{sh} is the radius of the black hole shadow, D is the distance of the centre of the black hole from the observer, 2α is the angular diameter. As the distance between the black hole and the observer is much greater than the radius of the black hole shadow, the small angle approximation is justified.

The mass and distance of M87* needs to be independently measured. The mass of M87* has been reported to be $M = 3.5_{-0.3}^{+0.9} \times 10^9 M_\odot$ from model gas dynamics mass measurements [83]. However, based on model stellar dynamics mass measurements, the mass is reported to be $M = 6.2_{-0.5}^{+1.1} \times 10^9 M_\odot$ [84, 85]. The distance of the gravitating source is reported to be $D = (16.8 \pm 0.8)\text{Mpc}$. Having the information of



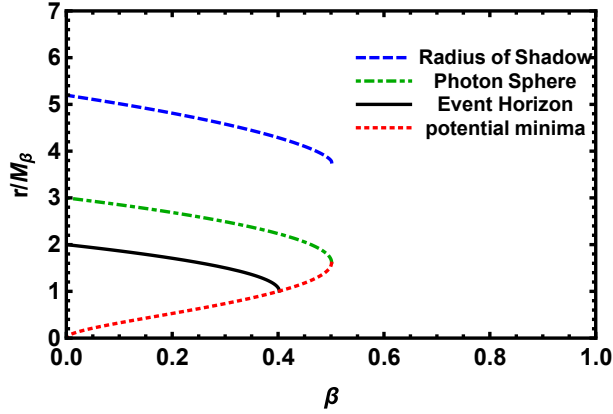
(a) Minima of the potential have been shown here. This corresponds to stable circular orbits. However, the relevance of the stable circular orbit is valid only for $\beta_{\text{crit}} < \beta \lesssim 0.5$



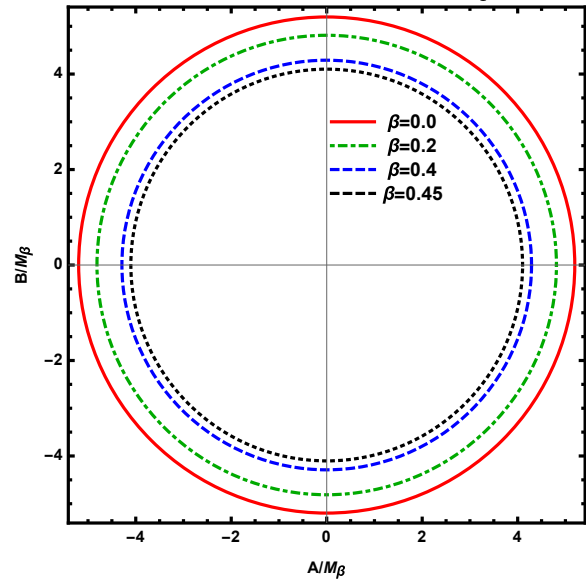
(b) Maxima of the potential have been shown here. This corresponds to the existence of the unstable circular orbits and is valid for the range $0 < \beta \lesssim 0.5$

Figure 2: The variation of the potential for the photon particle has been shown in these plots (a) minima of the potential has been shown and (b) maxima of the potential has been shown. For $\beta < \beta_{\text{crit}}$, there exists a stable circular orbit along with an unstable circular orbit. However, for the MOG static spherically symmetric solution only unstable circular orbits exist for $\beta < \beta_{\text{crit}}$. The existence of both stable and unstable circular orbits is possible for $\beta_{\text{crit}} < \beta \lesssim 0.5$.

mass and distance of the black hole one can define the angular gravitational radius $\theta = GM/c^2 D$. The angular gravitational radius θ_{dyn} as measured by stellar-dynamics process and the angular gravitational radius θ_g as reported by EHT are more or less consistent [86]. Theoretical bounds on the shadow diameter has been discussed by Kocherlakota et. al. [87] Based on M87* shadow size they have implied restrictions on the physical charges of several different spinning or non-rotating black holes. We use the stellar dynamics mass measurement to theoretically deduce the shadow radius of the black hole. The super-massive black hole M87* in the core of the galaxy M87 has an angular diameter of $(42 \pm 3) \mu\text{as}$, according



(a) Variation of various radii with variation of the parameter β .



(b) Variation of the shadow radius with variation of parameter β .

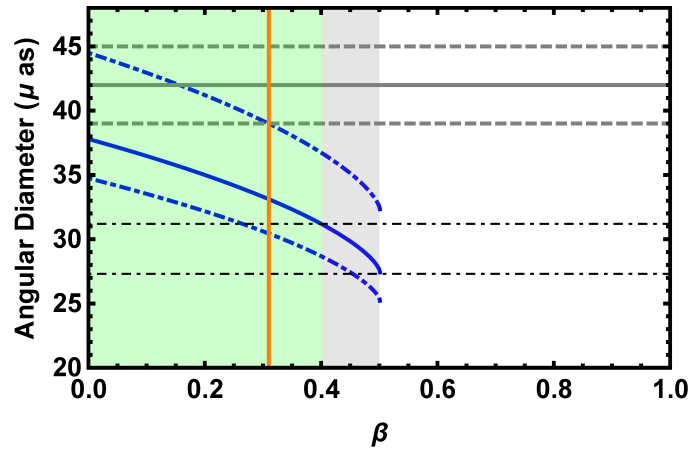
Figure 3: (a) The variation of the horizon radius, photon sphere and the radius of the shadow are depicted as a function of the parameter β . It is interesting to note that in the range $0.4 \lesssim \beta \lesssim 0.5$ there is no event horizon. However, this does not hinder us in defining the photon sphere and shadow for the compact object. Also, for the range of parameter space, we have both stable and unstable circular orbits. (b) The circular shadow structures have been depicted.

to the Event Horizon Telescope (EHT) collaboration [2]. In the plots shown in Fig. [4], the central value $42 \mu as$ second has been shown with a grey line and the error bar has been shown with the dashed grey line. There is an error in the mass estimation of M87* around the central value. The variation of angular

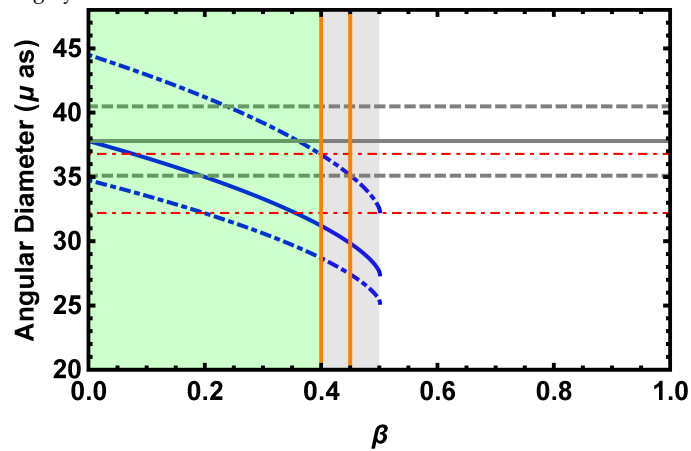
diameter, taking the central value of mass, has been shown with a blue line. Taking the errors, we can also plot the angular diameter. This has been shown with dot-dashed blue lines. The central value of mass of M87* is $6.2 \times 10^9 M_{\odot}$.

Considering the error bars both for angular diameter measurement and mass measurement, there is a possibility that M87* could be a regular MOG black hole. For the angular diameter $(42 \pm 3)\mu as$ the value of the parameter β can be as high as approximately $\beta = 0.3$. This has been shown with a vertical orange line in Fig. [4a]. So, in this case we can say that the M87* is a regular MOG black hole. With the angular diameter $(42 \pm 3)\mu as$, the possibility that M87* is a horizonless compact object can be rejected. However, if one considers a 10% offset value of the angular diameter, the parameter β can be as high as approximately $\beta = 0.45$, and in this case M87* can be a horizonless compact object. In Fig. [4b], the theoretical range of β has been shown by a grey shaded region and the region enclosed by the two orange lines in grey shaded represents the observationally allowed range of the parameter β for M87*.

According to the EHT collaboration, the angular diameter of the Sgr A* shadow is $(48.7 \pm 7)\mu as$ [88–93]. The angular diameter of the Sgr A* shadow depends on the determined mass and distance of Sgr A*. Several groups have reported the mass and distance of Sgr A*. From the Keck team, keeping the redshift parameter free the mass and distance of Sgr A* have been reported to $(3.975 \pm 0.058 \pm 0.026) \times 10^6 M_{\odot}$ and $(7959 \pm 59 \pm 32)pc$, respectively [94]. The same group has also reported the mass and distance assuming the redshift parameter to be unity and these are $(3.951 \pm 0.047) \times 10^6 M_{\odot}$ and $(7935 \pm 50)pc$, respectively [94]. The mass and distance, according to the Gravity collaboration are, respectively, $(4.261 \pm 0.012) \times 10^6 M_{\odot}$ and $(8246.7 \pm 9.3)pc$ [95, 96]. The Gravity Collaboration further limited the BH mass $(4.297 \pm 0.012 \pm 0.040) \times 10^6 M_{\odot}$ and the distance $(8277 \pm 9 \pm 33)pc$ by accounting for optical aberrations. In Fig. [5], we have plotted the angular diameter as a function of the parameter β with mass and distance as given by the above teams. From the plot, using the Keck team data, one can constrain the parameter to be $0 < \beta \lesssim 0.4$. With the Keck team data, it is almost impossible to say that Sgr A* is a horizonless compact object. However, using the Gravity collaboration data, we can say that there is a possibility that Sgr A* is a horizonless compact object, because with the Gravity collaboration data the parameter range is $0 < \beta \lesssim 0.46$.



(a) Angular diameter versus β with observed values $(42 \pm 3) \mu as$ marked in grey



(b) Angular diameter versus β with observed values $(37.8 \pm 2.7) \mu as$ marked in grey

Figure 4: (a) The variation of the ring diameter has been shown with the error bar. (b) The variation of the shadow diameter has been shown.

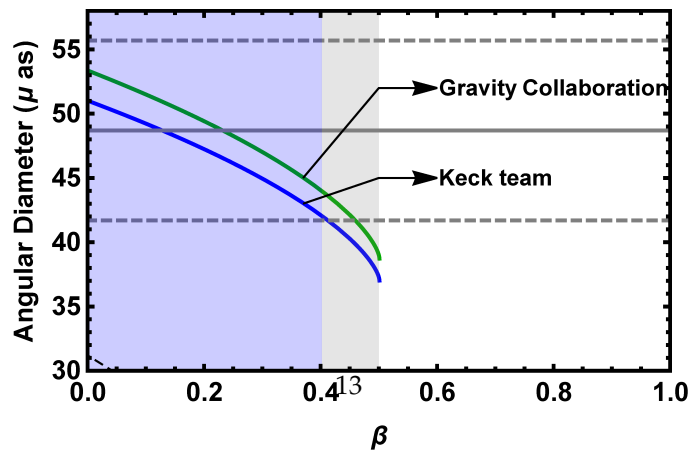


Figure 5: Theoretical angular diameter for Sgr A* has been shown.

5 Regular MOG rotating compact object

The regular rotating MOG solution can be obtained with the help of the modified Newman-Janis algorithm. The associated line element of the spacetime in Boyer-Lindquist coordinates is given by [81]

$$ds^2 = -f(r, \theta) dt^2 - 2a \sin^2 \theta \{1 - f(r, \theta)\} d\phi dt + \frac{\Sigma}{\Delta} dr^2 + \Sigma d\theta^2 + \sin^2 \theta [\Sigma - a^2 \{f(r, \theta) - 2\} \sin^2 \theta] d\phi^2 \quad (40)$$

where

$$f(r, \theta) = 1 - \frac{2M_\beta r \sqrt{\Sigma}}{[\Sigma + \beta M_\beta^2]^{3/2}} + \frac{\beta M_\beta^2 \Sigma}{[\Sigma + \beta M_\beta^2]^2} \quad (41a)$$

$$\Delta = \Sigma f(r, \theta) + a^2 \sin^2 \theta \quad (41b)$$

$$\Sigma = r^2 + a^2 \cos^2 \theta \quad (41c)$$

Here, M_β is the ADM mass of the spacetime, β is the enhancement parameter and a is the spin parameter. A certain portion of the full parameter space of $\beta - a$ is available for the existence of the regular rotating MOG black hole. The parameter space has been shown in Fig. [6]. From the figure, it is noticeable that the highly spinning regular MOG black hole has a relatively low value of the parameter β .

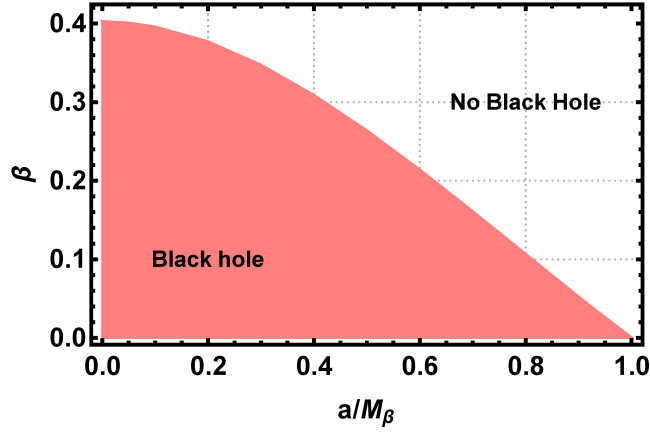


Figure 6: Parameter space of $(\beta - a)$ plane for the regular rotating MOG solution is displayed here. The reddish region represents the black hole solution and the boundary denotes the occurrence of an extremal black hole.

The location and the structure of the static limit surface are obtained by setting the prefactor of dt^2 to zero. The SLS can be determined by solving the following equation

$$(\Sigma + \beta M_\beta^2)^2 - 2M_\beta r \sqrt{\Sigma(\Sigma + \beta M_\beta^2)} + \beta M_\beta^2 \Sigma = 0 \quad (42)$$

For $\beta = 0$, we have the usual Kerr scenario. The variation and existence of the static limit surface for rotating regular MOG black holes has been displayed in Fig. [7]. The location of the horizon is determined

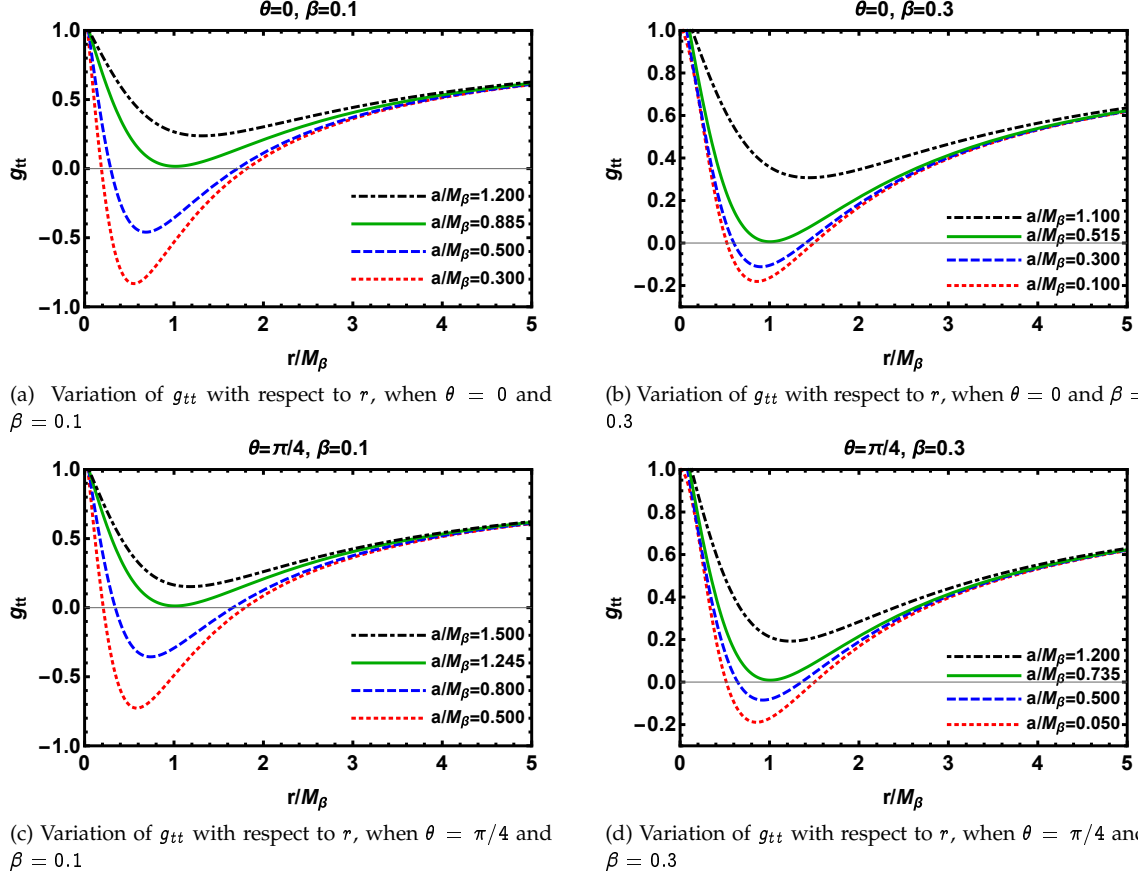


Figure 7: The nature of the static limit surface (SLS) has been depicted as a function of coordinate r for various values of spin parameter a . The variation of the SLS with respect to the enhancement parameter β can be seen along the row of the figure matrix [i.e (a)-(b) and (c)-(d)]

by setting the g^{rr} to be zero, which in turn gives

$$\Delta = \Sigma f(r, \theta) + a^2 \sin^2 \theta = 0 \quad (43)$$

The existence of the horizon in the regular rotating MOG solution has been depicted in Fig. [8].

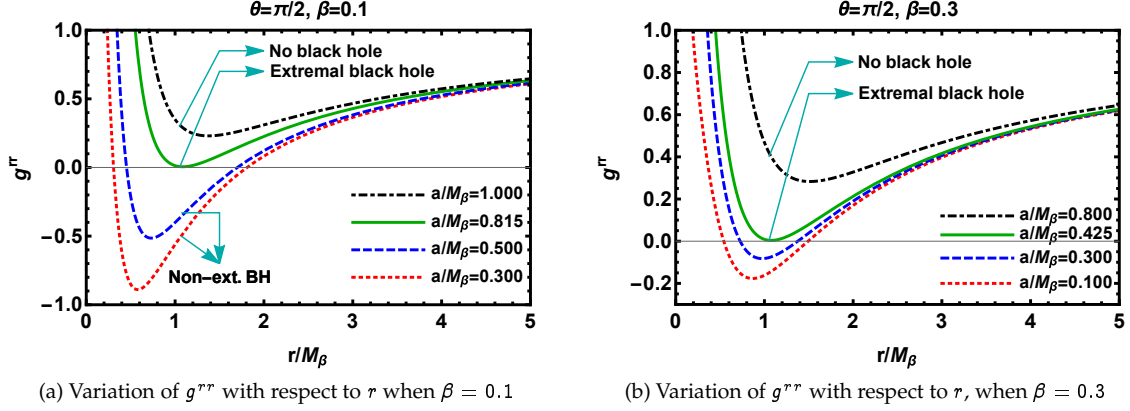


Figure 8: A set of parameter values are allowed for black hole solutions. In these plots, the set of parameters has been shown for the extremal black hole. The horizonless compact object can result for an increase in spin keeping the enhancement parameter β constant. (a) The enhancement parameter β is 0.1. Whereas in (b) the enhancement parameter is 0.3.

6 Analysis of the black hole shadow

To investigate the black hole shadow, we must determine the photon geodesic equations for the metric given in Eq. (40). When using the Hamilton-Jacobi formulation for the rotating MOG regular solution, it is particularly challenging to separate the equations, since the function $f(r, \theta)$ has a highly complex structure. Consequently, to overcome this issue, we consider an approximation for θ , such that $\theta \approx \pi/2 + \epsilon$. [97] Note that although we are focusing on photon orbits that are close to the equator, unstable photon circular orbits are not only limited to this region. This fact does not invalidate the calculations that follow, because the major goal of this work is to calculate the shadow of a black hole cast by an observer at infinity, which can be done using the approximations indicated above. The trigonometric functions here have the following form: $\sin \theta \approx 1$ and $\cos \theta \approx -\epsilon$. With these approximations the function $f(r, \theta)$ becomes $f(r)$, which is given by

$$f(r) = 1 - \frac{2M_\beta r^2}{(r^2 + \beta M_\beta^2)^{3/2}} + \frac{\beta M_\beta^2 r^2}{(r^2 + \beta M_\beta^2)^2} \quad (44)$$

6.1 Null geodesics

For a general stationary, axisymmetric metric the Lagrangian \mathcal{L} can be written as

$$g_{\mu\nu} \dot{x}^\mu \dot{x}^\nu = g_{tt} \dot{t}^2 + 2g_{t\phi} \dot{t} \dot{\phi} + g_{\phi\phi} \dot{\phi}^2 + g_{rr} \dot{r}^2 + g_{\theta\theta} \dot{\theta}^2 = 2\mathcal{L} \quad (45)$$

For massive particles and massless particles, the Lagrangian is equal to unity and zero, respectively. The associated Hamiltonian is provided by

$$\mathcal{H} = p_\mu \dot{x}^\mu - \mathcal{L} = \frac{1}{2} g^{\mu\nu} p_\mu p_\nu = \frac{k}{2} \quad (46)$$

with k , which in this instance is zero and represents the test particle's rest mass. By utilising the Hamilton-Jacobi technique, we may connect the Hamiltonian to the action S by

$$\mathcal{H}(x^\mu, p^\mu) + \frac{\partial S}{\partial \lambda} = 0 \quad \text{with} \quad p_\mu = \frac{\partial S}{\partial x^\mu} \quad (47)$$

The metric described in Eq. (45) is independent of t and ϕ , whereby the (specific) energy E and the (specific) angular momentum L are conserved quantities. These are supplied by

$$E = g_{tt} \dot{t} + g_{t\phi} \dot{\phi} \quad (48a)$$

$$L = g_{t\phi} \dot{t} + g_{\phi\phi} \dot{\phi} \quad (48b)$$

From the aforementioned context, the action may be expressed as

$$S = -Et + L\phi + S(r, \epsilon) \quad (49)$$

Now, for the metric given in Eq. (40), Eq. (49) is separable such that $S(r, \theta) = S_r(r) + S_\epsilon(\epsilon)$. Substituting Eq. (49) in equation Eq. (46) we get

$$g^{rr} \left(\frac{\partial S^r}{\partial r} \right)^2 + g^{\theta\theta} \left(\frac{\partial S^\theta}{\partial \theta} \right)^2 + g^{tt} (-E)^2 + 2g^{t\phi} (-E)L + g^{\phi\phi} L^2 = 0 \quad (50)$$

The metric in Eq. (40) causes the equation above to take the form:

$$\Delta \left(\frac{dS^r}{dr} \right)^2 + \left(\frac{dS^\epsilon}{d\epsilon} \right)^2 - \left\{ \frac{1}{\Delta} [r^2 + a^2]^2 - a^2 \right\} E^2 + \frac{2ar^2}{\Delta} \{1 - f(r)\} EL + \frac{r^2 f(r)}{\Delta} L^2 = 0 \quad (51)$$

It's interesting to note that the r and θ components of the preceding equation may be split up so that

$$\Delta \left(\frac{dS^r}{dr} \right)^2 - \frac{1}{\Delta} [r^2 + a^2]^2 E^2 + \frac{2ar^2}{\Delta} \{1 - f(r)\} EL + \frac{r^2 f(r)}{\Delta} L^2 + a^2 E^2 = - \left(\frac{dS^\epsilon}{d\epsilon} \right)^2 = -C \quad (52)$$

The Carter constant is represented by C . The left-hand side of Eq. (52) is only a function of r , whereas the right-hand side is a function of θ alone. The radial component of Eq. (52) may be expressed as

$$\left[\frac{dS^r}{dr} \right]^2 = \frac{R(r)}{\Delta^2} \quad (53)$$

where

$$R(r) = -\Delta [C + (L - aE)^2] + \{[r^2 + a^2] E - aL\}^2 \quad (54)$$

The angular part can be written as

$$\left(\frac{dS^\epsilon}{d\epsilon}\right)^2 = C \quad (55)$$

Consequently, the action adopts the form

$$S = -Et + L\phi + \int \frac{\sqrt{R(r)}}{\Delta} dr + \int \sqrt{C} d\epsilon \quad (56)$$

The equation of motion for r and ϵ is given by

$$\dot{r} = \pm \frac{\sqrt{R}}{r^2} \quad (57)$$

$$\dot{\epsilon} = \pm \frac{\sqrt{C}}{r^2} \quad (58)$$

For determining the unstable circular orbits, one needs to introduce $\chi = \frac{C}{E^2}$ and $\eta = \frac{L}{E}$. The unstable circular orbit can be obtained by setting $R(r) = 0 = \frac{dR(r)}{dr}$. So, using Eq. (54) with aforementioned conditions one obtains

$$[r^2 f(r) + a^2] (\chi + \eta^2 + a^2 - 2\eta a) = [r^2 + a^2 - a\eta]^2 \quad (59)$$

$$\chi + \eta^2 + a^2 - 2\eta a = \frac{4}{[2f(r) + rf'(r)]} [r^2 + a^2 - a\eta] \quad (60)$$

These two equations can be solved to get two one-parameter classes of solutions parametrized in terms of r , which is the radius of unstable circular orbits:

(i)

$$\chi = -\frac{r^4}{a^2} \quad (61)$$

$$\eta = \frac{a^2 + r^2}{a} \quad (62)$$

(ii)

$$\chi = \frac{r^3 [8a^2 f'(r) - r \{rf'(r) - 2f(r)\}^2]}{a^2 \{rf'(r) + 2f(r)\}^2} \quad (63)$$

$$\eta = \frac{1}{a} \left[r^2 + a^2 - \frac{4(r^2 f(r) + a^2)}{2f(r) + rf'(r)} \right] \quad (64)$$

The solution of the first kind is not a physical solution, but the second solution helps to determine the contour of the shadow in the (η, χ) plane. Further, this solution satisfies the following condition for the critical curve:

$$a^2 - \chi - \eta^2 = \frac{8(a^2 + r^2 f(r))}{rf'(r) + 2f(r)} - \frac{16(a^2 + r^2 f(r))}{(rf'(r) + 2f(r))^2} - 2r^2 \quad (65)$$

When we consider the non-rotating case i.e the regular MOG static spherically symmetric solution, we have

$$\chi + \eta^2 = \frac{2r_{ph}^2 [4f(r_{ph})^2 - 8f(r_{ph}) - r_{ph}^2 f'(r_{ph})^2]}{\{r_{ph} f'(r_{ph}) + 2f(r_{ph})\}^2} \quad (66)$$

Here, r_{ph} is the radius of the photon sphere. The above equation helps to find the shadow of the regular MOG static, spherically symmetric solution.

6.2 Celestial coordinates and shadow structure

We now want to find out how the rotating MOG regular black hole shadow appears to be shaped. For a clearer depiction, we locate the shadow using the celestial coordinates A_i and B_i . These coordinates are introduced as

$$A_i = \lim_{r_0 \rightarrow \infty} \left(-r_0^2 \sin \theta_0 \frac{d\phi}{dr} \right) \quad (67)$$

$$B_i = \lim_{r_0 \rightarrow \infty} \left(r_0^2 \frac{d\epsilon}{dr} \right) \quad (68)$$

where r_0 is the distance between the black hole and the distant observer and θ_0 is the inclination angle i.e the angle between the line of sight and the rotation axis of the black hole. From further calculations and considering the limit, one can arrive at the following:

$$A_i = -\eta \quad (69)$$

$$B_i = \sqrt{\chi} \quad (70)$$

The photons are now parametrized by the conserved quantities (η, χ) . All the light rays, coming from the source placed behind the black hole, will not be able to reach the observer as the black hole will hinder a portion of light rays due to gravitational lensing as shown in Fig. [9]. The dark patch that appears to the observer is known as the black hole shadow and the boundary of this shadow can be determined allowing the parameters (η, χ) all possible values. The coordinates A_i and B_i are known as celestial coordinates. For a spherically symmetric scenario, these coordinates do not depend on the inclination angle and the shadow appears to be a perfect circle. However, the inclusion of the rotational effect of compact objects and the inclination angle make the shadow dented and not a perfect circle. The shape and size of the shadow can be analysed to determine the parameters including the spin parameter of the black hole. The variation of the shape and size of the black hole shadow has been depicted in Fig. [10].

6.3 Observables

For further analysis of the shape of the critical curve, we are going to define two new observables as prescribed by Hioki and Maeda [98]. To define these observables, we need to characterize a few points of the critical curve while fitting it with a circular outline. Consider a circle in Fig. [11] that passes through the three extreme points of the shadow curve. The points are:

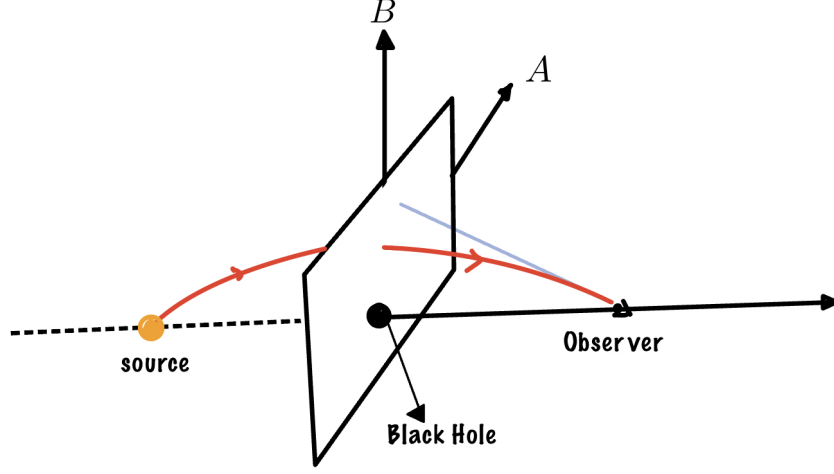


Figure 9: Schematic diagram of lensing and formation of shadow

- extreme right of the shadow i.e $U(A_r, 0)$, at which the shadow intersects the A – axis.
- top-most point of the shadow i.e $V(A_t, B_t)$
- bottom-most point of the shadow i.e $W(A_b, B_b)$

As the shape of the shadow is not circular, the extreme left point of the shadow does not coincide with the extreme left point of the associated circle. This characterizes the distortion of the shape of the shadow from a circular shape. The extreme left point of the shadow is $P(A_l, 0)$ and the extreme point of the associated circle is $Q(A_L, 0)$. Now we define the two observables associated with the shadow curve, which are

- (i) The characteristic radius R_s , which can be defined as

$$R_s = \frac{(A_t - A_r)^2 + B_t^2}{2|A_t - A_r|} \quad (71)$$

- (ii) Distortion parameter δ_s , which is defined as

$$\delta_s = \frac{D_s}{R_s} = \frac{|A_L - A_l|}{R_s} \quad (72)$$

For a non-rotating scenario, the distortion parameter becomes zero as the shape of the shadow for such a case is always zero. Similarly, the characteristic radius reduces to the radius of the circle for the non-rotating scenario. So these two observables measure the deviation from the circularity of the shape of the

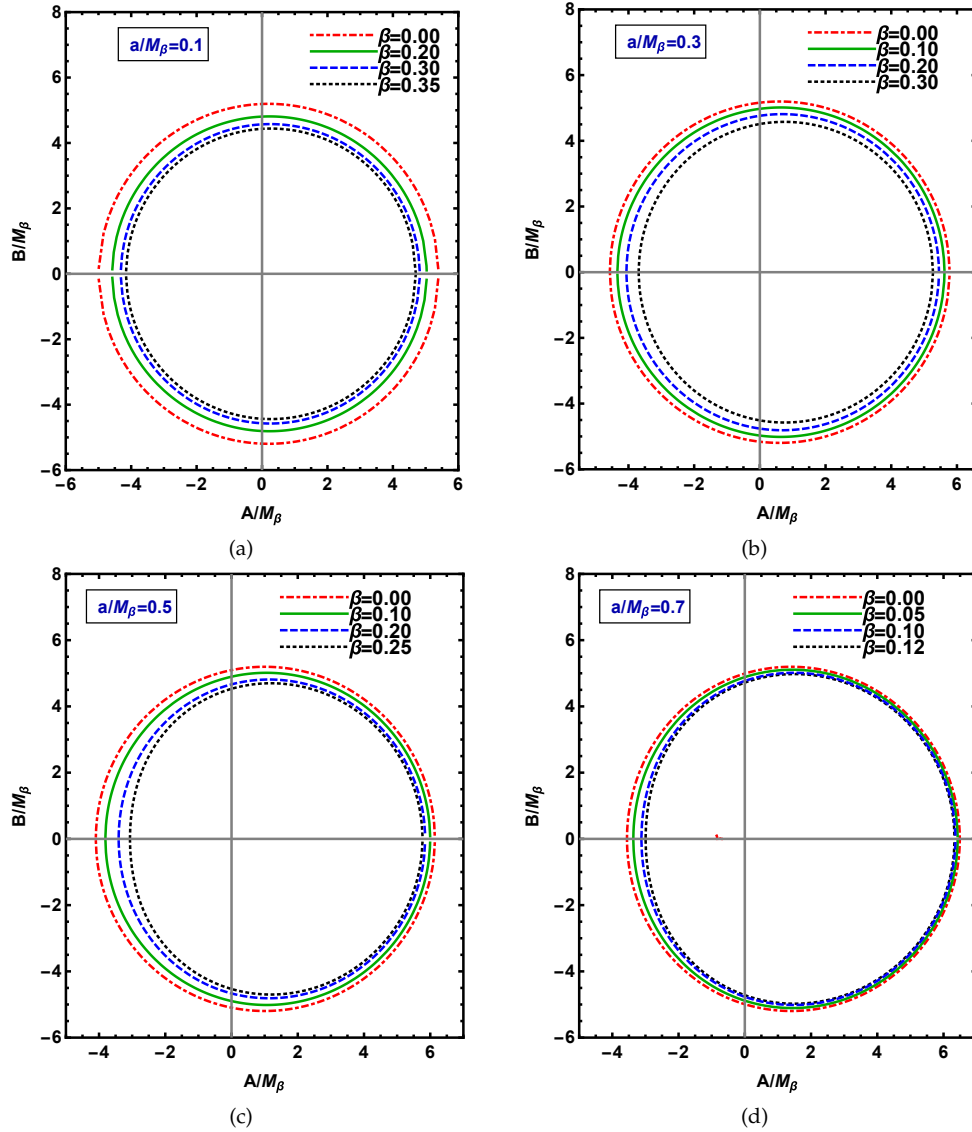


Figure 10: Shadow of the regular MOG rotating black hole is situated at the origin of the coordinate system. The inclination angle is $\theta_0 = \pi/2$. Each image represents the shadow for a fixed value of the spin parameter a . One can note that just like in the Kerr scenario, here also the shadow gets dented with an increase in spin parameter a . An increase in the parameter β causes a shrinking of the shadow for a fixed value of the spin parameter.

shadow. It has been illustrated in Fig. [12] how the parameter β affects the characteristic radius R_s and distortion parameter δ_s of the spinning regular MOG black hole. The change in the observables has been

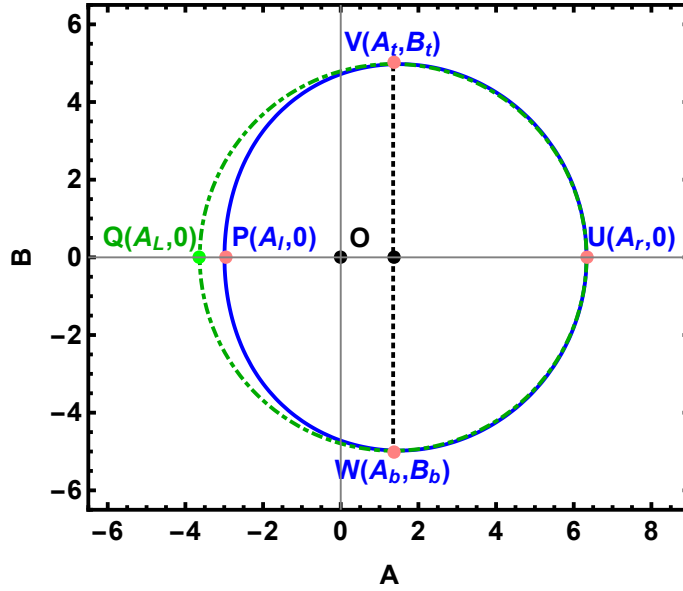


Figure 11: Characteristic points have been shown in the schematic diagram of the black hole shadow. A solid blue curve is the outline of the black hole shadow. The dot-dashed green curve is associated with the fitting circle. The associated circle passes through the three points of the shadow outline. The top-most and bottom-most points of the shadow are, respectively, V and W . The left-most and right-most points of the shadow outline are P and U . A separation distance of points P and Q measures the distortion parameter δ_s .

shown for two fixed values of the spin parameters a .

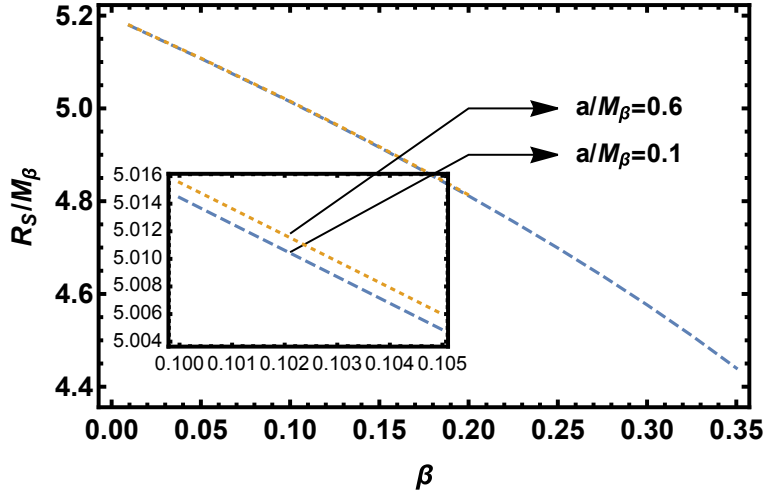
7 Energy emission rate for the rotating regular MOG black hole

For the regular rotating MOG solution, the observers see the large energy absorption cross-section is caused by the shadows of black holes. At high energies, the black hole absorption cross sections exhibit a little modulation close to a limiting constant value. We may use the absorption cross-section limiting constant value for a nearly spherically symmetric black hole as a decent approximation, which is given by

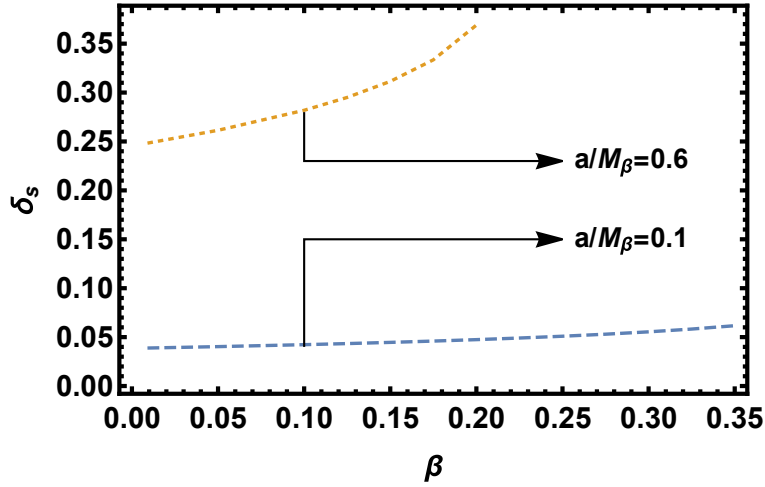
$$\sigma_{lim} \approx \pi R_s^2 \quad (73)$$

The energy emission rate of the concerned black hole is given as [99]:

$$\frac{d^2 E(\omega)}{d\omega dt} = \frac{2\pi^3 R_s^2 \omega^3}{e^{\omega/T} - 1} \quad (74)$$



(a) Variation of R_s with β



(b) Variation of δ_s with β

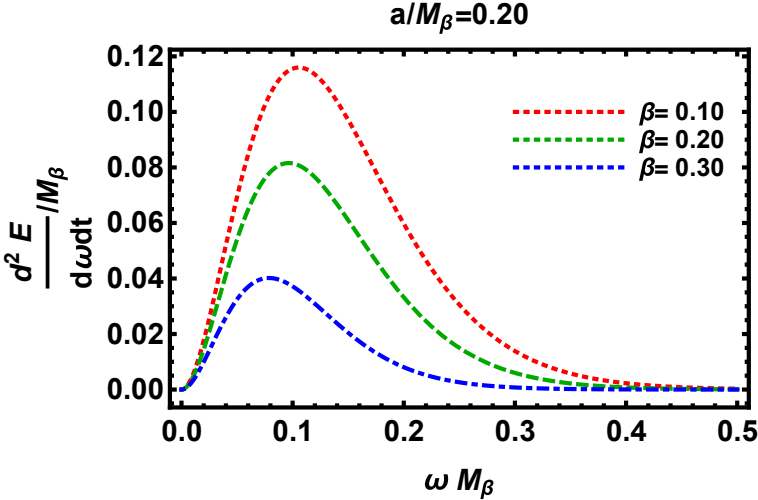
Figure 12: The variation of characteristic radius R_s and distortion parameter δ_s of the regular rotating MOG black hole as a function of parameter β has been shown. The variation has been shown for a fixed value of spin parameter a . From the plots, one notices how the observables get changed with the spin parameter.

where ω is the frequency of the photon and T is the Hawking temperature, which can be defined as [99]:

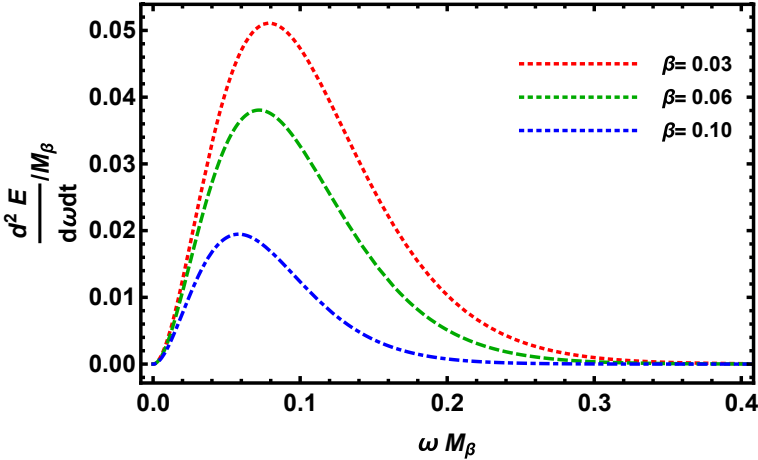
$$T = \lim_{\theta=0, r \rightarrow r_+} \frac{\partial_r \sqrt{-g_{tt}}}{2\pi \sqrt{g_{rr}}} \quad (75)$$

Here, r_+ is the outer event horizon of the regular rotating MOG black hole. In Fig. [13], we have plotted the energy emission rate of the black hole with the frequency of the photon ω for different values of the

parameter β . One notices from the figure that the peak of the energy emission rate shifts towards a lower frequency as the parameter β increases.



(a) Energy emission rate for the value of spin parameter $a/M_\beta = 0.20$



(b) Energy emission rate for the value of the spin parameter $a/M_\beta = 0.80$

Figure 13: Energy emission rate as a function of frequency has been shown. For a fixed value of the spin parameter, the increase in the parameter β causes a shift of the peak of the spectrum to a lower frequency.

8 Conclusions

In this paper, we have explored the regular black hole solution in STVG/MOG theory. In early papers on this theory, the parameter space is from zero to infinity. We have compactified the range of the parameter space with a modification of the form of the parameter β . At first, we have focused on the regular solution of STVG/MOG theory in the static, spherically symmetric scenario and also determined analytically the critical value of the parameter β . For the dimensionless parameter $\beta \lesssim 0.4$, we have a black hole solution with two horizons in the spherically symmetric case. For $0.4 \lesssim \beta \lesssim 0.5$, there is no black hole solution as there exists no horizon. For the critical value of the parameter $\beta \cong 0.40263$, a single horizon black hole solution can be obtained. We have also studied the null geodesics in this spacetime as it is a prerequisite to analyse the shadow of the black hole. For $\beta < \beta_{\text{crit}}$, only unstable circular orbits exist. However, for $\beta_{\text{crit}} < \beta \lesssim 0.5$, there exists a stable circular orbit. It is also noticeable that the radius of the photon sphere, the radii of the shadow and the event horizon decrease as the parameter β increases. Thus, the circular shadow shrinks as the parameter β is increased. Furthermore, as the shadows of M87* and Sgr A* are more or less circular in shape, we have tried to compare the theoretical outcomes with the observational data. For this purpose, we have used independent mass measurements to calculate the theoretical angular diameter. The regular MOG black holes and the possibility of horizonless compact objects are compatible with the EHT data and mass measurements.

We have considered the regular rotating MOG black hole by studying the behaviours of the horizon and static limit surface for a change in the parameter β . Just like the spherically symmetric case, here also a critical value of parameter β exists for a fixed value of the spin parameter a . We have determined the parameter space for which a rotating regular black hole exists. As a chief goal of this paper, a special emphasis has been placed on the black hole shadow. However, we have considered only equatorial approximations. How the shape and size of the associated shadow transforms have been determined. As the spin parameter, a , increases the shape gets more deformed from a circular shape. The increasing value of parameter β causes the size of the shadow to become smaller. To analyse the shadow, the required observables have been defined and plotted. One of the observables has been used to evaluate the energy emission rate for the rotating regular MOG black hole. From this, we have concluded that the peak of the energy emission rate shifts to a lower frequency for a relatively large value of the parameter β .

It is hard to decouple the differential equations in terms of r and θ without an equatorial approximation. We have reported the analysis of shadows using numerical techniques, using the observables as introduced by Hioki and Maeda. However, one can introduce new observables or can use other existing observables to study the shadows.

In this work, we have demonstrated that classical regular black holes and regular horizonless dark compact objects, generally considered to be distinct families of astrophysical objects, are a family of connected astrophysical objects continuously deformed into one another, depending on the range and value of the parameter β . Our work illustrates that different strong gravity geometries describe alternative states of black holes and compact astrophysical objects in their lifetime. It is expected that at the small scale reached at the central value of the compact object when $r \rightarrow 0$, quantum gravity will take over [100]. The regular and horizonless compact objects derived from the MOG field equations in this work are classical in nature. The stability of photon orbits around the black hole and dark compact object shadows will produce viability issues for the existence of these astrophysical objects. For the MOG-Schwarzschild

and MOG-Kerr solutions with two horizons, the inner Cauchy horizon can lead to instability problems.

In future work, the gravitational collapse of stars will be investigated, assuming a form of matter and stress-energy, by solving the time dependent MOG field equations. Moreover, the merging of the regular and horizonless dark compact objects, producing gravitational waves and the subsequent ring-down phase, will be investigated. Singularity-resolving physics in photon rings can further be studied in context of MOG theory [101].

Acknowledgement

Research at the Perimeter Institute is supported by the Government of Canada through the Department of Innovation, Science and Economic Development Canada and by the Province of Ontario through the Ministry of Research, Innovation and Science.

References

- [1] **Event Horizon Telescope** Collaboration, V. L. Fish, K. Akiyama, K. L. Bouman, A. A. Chael, M. D. Johnson, S. S. Doeleman, L. Blackburn, J. F. C. Wardle, and W. T. Freeman, “Observing—and Imaging—Active Galactic Nuclei with the Event Horizon Telescope,” *Galaxies* **4** no. 4, (2016) 54, [arXiv:1607.03034 \[astro-ph.IM\]](#).
- [2] **Event Horizon Telescope** Collaboration, K. Akiyama *et al.*, “First M87 Event Horizon Telescope Results. I. The Shadow of the Supermassive Black Hole,” *Astrophys. J. Lett.* **875** (2019) L1, [arXiv:1906.11238 \[astro-ph.GA\]](#).
- [3] **Event Horizon Telescope** Collaboration, K. Akiyama *et al.*, “First M87 Event Horizon Telescope Results. II. Array and Instrumentation,” *Astrophys. J. Lett.* **875** no. 1, (2019) L2, [arXiv:1906.11239 \[astro-ph.IM\]](#).
- [4] **Event Horizon Telescope** Collaboration, K. Akiyama *et al.*, “First M87 Event Horizon Telescope Results. III. Data Processing and Calibration,” *Astrophys. J. Lett.* **875** no. 1, (2019) L3, [arXiv:1906.11240 \[astro-ph.GA\]](#).
- [5] **Event Horizon Telescope** Collaboration, K. Akiyama *et al.*, “First M87 Event Horizon Telescope Results. IV. Imaging the Central Supermassive Black Hole,” *Astrophys. J. Lett.* **875** no. 1, (2019) L4, [arXiv:1906.11241 \[astro-ph.GA\]](#).
- [6] **Event Horizon Telescope** Collaboration, K. Akiyama *et al.*, “First M87 Event Horizon Telescope Results. V. Physical Origin of the Asymmetric Ring,” *Astrophys. J. Lett.* **875** no. 1, (2019) L5, [arXiv:1906.11242 \[astro-ph.GA\]](#).
- [7] **Event Horizon Telescope** Collaboration, K. Akiyama *et al.*, “First M87 Event Horizon Telescope Results. VI. The Shadow and Mass of the Central Black Hole,” *Astrophys. J. Lett.* **875** no. 1, (2019) L6, [arXiv:1906.11243 \[astro-ph.GA\]](#).

- [8] **LIGO Scientific, Virgo Collaboration**, B. P. Abbott *et al.*, “Observation of Gravitational Waves from a Binary Black Hole Merger,” *Phys. Rev. Lett.* **116** no. 6, (2016) 061102, [arXiv:1602.03837](https://arxiv.org/abs/1602.03837) [gr-qc].
- [9] **LIGO Scientific, Virgo Collaboration**, R. Abbott *et al.*, “GW190412: Observation of a Binary-Black-Hole Coalescence with Asymmetric Masses,” *Phys. Rev. D* **102** no. 4, (2020) 043015, [arXiv:2004.08342](https://arxiv.org/abs/2004.08342) [astro-ph.HE].
- [10] **LIGO Scientific Collaboration and Virgo Collaboration** Collaboration, R. A. *et al.*, “Gw190521: A binary black hole merger with a total mass of $150 M_{\odot}$,” *Phys. Rev. Lett.* **125** (Sep, 2020) 101102. <https://link.aps.org/doi/10.1103/PhysRevLett.125.101102>.
- [11] R. Geroch, “What is a singularity in general relativity?,” *Annals of Physics* **48** no. 3, (1968) 526–540. <https://www.sciencedirect.com/science/article/pii/0003491668901449>.
- [12] E. T. NEWMAN and R. POSADAS, “Motion and structure of singularities in general relativity,” *Phys. Rev.* **187** (Nov, 1969) 1784–1791. <https://link.aps.org/doi/10.1103/PhysRev.187.1784>.
- [13] A. J. C. de Souza, “Introductory chapter: The physics of dark sector,” in *Essentials on Dark Matter*, A. J. C. de Souza, ed., ch. 1. IntechOpen, Rijeka, 2018. <https://doi.org/10.5772/intechopen.80234>.
- [14] N. C. Martens and D. Lehmkuhl, “Dark matter = modified gravity? scrutinising the spacetime–matter distinction through the modified gravity/ dark matter lens,” *Studies in History and Philosophy of Science Part B: Studies in History and Philosophy of Modern Physics* **72** (2020) 237–250. <https://www.sciencedirect.com/science/article/pii/S135521982030109X>.
- [15] S. Nojiri and S. D. Odintsov, “Is the future universe singular: Dark matter versus modified gravity?,” *Physics Letters B* **686** no. 1, (2010) 44–48. <https://www.sciencedirect.com/science/article/pii/S0370269310001917>.
- [16] X. Calmet and I. Kuntz, “What is modified gravity and how to differentiate it from particle dark matter?,” *Eur. Phys. J. C* **77** no. 2, (2017) 132, [arXiv:1702.03832](https://arxiv.org/abs/1702.03832) [gr-qc].
- [17] R. H. Sanders, “Modified gravity without dark matter,” *Lect. Notes Phys.* **720** (2007) 375–402, [arXiv:astro-ph/0601431](https://arxiv.org/abs/astro-ph/0601431).
- [18] S. Nojiri and S. D. Odintsov, “Dark energy, inflation and dark matter from modified F(R) gravity,” *TSPU Bulletin* **N8(110)** (2011) 7–19, [arXiv:0807.0685](https://arxiv.org/abs/0807.0685) [hep-th].
- [19] S. Nojiri and S. D. Odintsov, “Modified gravity as realistic candidate for dark energy, inflation and dark matter,” *AIP Conf. Proc.* **1115** no. 1, (2009) 212–217, [arXiv:0810.1557](https://arxiv.org/abs/0810.1557) [hep-th].
- [20] L. Baudis, “The search for dark matter,” *European Review* **26** no. 1, (2018) 70–81.
- [21] J. Liu, X. Chen, and X. Ji, “Current status of direct dark matter detection experiments,” *Nature Phys.* **13** no. 3, (2017) 212–216, [arXiv:1709.00688](https://arxiv.org/abs/1709.00688) [astro-ph.CO].

- [22] J. W. Moffat, “Scalar-tensor-vector gravity theory,” *JCAP* **03** (2006) 004, [arXiv:gr-qc/0506021](#).
- [23] J. W. Moffat, “Scalar and Vector Field Constraints, Deflection of Light and Lensing in Modified Gravity (MOG),” [arXiv:1410.2464 \[gr-qc\]](#).
- [24] Z. Davari and S. Rahvar, “MOG cosmology without dark matter and the cosmological constant,” *Mon. Not. Roy. Astron. Soc.* **507** no. 3, (2021) 3387–3399, [arXiv:2108.00266 \[astro-ph.CO\]](#).
- [25] J. W. Moffat and S. Rahvar, “The MOG weak field approximation and observational test of galaxy rotation curves,” *Monthly Notices of the Royal Astronomical Society* **436** no. 2, (09, 2013) 1439–1451, <https://academic.oup.com/mnras/article-pdf/436/2/1439/3933595/stt1670.pdf>.
<https://doi.org/10.1093/mnras/stt1670>.
- [26] J. W. Moffat and V. T. Toth, “Rotational velocity curves in the Milky Way as a test of modified gravity,” *Phys. Rev. D* **91** no. 4, (2015) 043004, [arXiv:1411.6701 \[astro-ph.GA\]](#).
- [27] J. W. Moffat and S. Rahvar, “The MOG weak field approximation and observational test of galaxy rotation curves,” *Mon. Not. Roy. Astron. Soc.* **436** (2013) 1439–1451, [arXiv:1306.6383 \[astro-ph.GA\]](#).
- [28] J. R. Brownstein and J. W. Moffat, “The Bullet Cluster 1E0657-558 evidence shows Modified Gravity in the absence of Dark Matter,” *Mon. Not. Roy. Astron. Soc.* **382** (2007) 29–47, [arXiv:astro-ph/0702146](#).
- [29] J. W. Moffat and S. Rahvar, “The MOG weak field approximation – II. Observational test of Chandra X-ray clusters,” *Monthly Notices of the Royal Astronomical Society* **441** no. 4, (06, 2014) 3724–3732, <https://academic.oup.com/mnras/article-pdf/441/4/3724/4059513/stu855.pdf>.
<https://doi.org/10.1093/mnras/stu855>.
- [30] J. W. Moffat, “Structure Growth and the CMB in Modified Gravity (MOG),” [arXiv:1409.0853 \[astro-ph.CO\]](#).
- [31] J. W. Moffat and V. T. Toth, “Modified Gravity: Cosmology without dark matter or Einstein’s cosmological constant,” [arXiv:0710.0364 \[astro-ph\]](#).
- [32] J. W. Moffat and V. T. Toth, “Cosmological observations in a modified theory of gravity (MOG),” *Galaxies* **1** (2013) 65–82, [arXiv:1104.2957 \[astro-ph.CO\]](#).
- [33] J. W. Moffat and V. Toth, “Scalar–Tensor–Vector Modified Gravity in Light of the Planck 2018 Data,” *Universe* **7** no. 10, (2021) 358, [arXiv:2104.12806 \[gr-qc\]](#).
- [34] S. Hu, C. Deng, D. Li, X. Wu, and E. Liang, “Observational signatures of Schwarzschild-MOG black holes in scalar-tensor-vector gravity: shadows and rings with different accretions,” *Eur. Phys. J. C* **82** no. 10, (2022) 885.

- [35] X. Qin, S. Chen, Z. Zhang, and J. Jing, “Polarized Image of a Rotating Black Hole in Scalar–Tensor–Vector–Gravity Theory,” *Astrophys. J.* **938** no. 1, (2022) 2, [arXiv:2207.12034](https://arxiv.org/abs/2207.12034) [gr-qc].
- [36] R. Della Monica, I. de Martino, and M. de Laurentis, “Orbital precession of the S2 star in Scalar–Tensor–Vector Gravity,” *Mon. Not. Roy. Astron. Soc.* **510** no. 4, (2022) 4757–4766, [arXiv:2105.12687](https://arxiv.org/abs/2105.12687) [gr-qc].
- [37] J. W. Moffat and V. T. Toth, “Masses and shadows of the black holes Sagittarius A* and M87* in modified gravity,” *Phys. Rev. D* **101** no. 2, (2020) 024014, [arXiv:1904.04142](https://arxiv.org/abs/1904.04142) [gr-qc].
- [38] A. Einstein, “Lens-like action of a star by the deviation of light in the gravitational field,” *Science* **84** no. 2188, (1936) 506–507, <https://www.science.org/doi/pdf/10.1126/science.84.2188.506>, <https://www.science.org/doi/abs/10.1126/science.84.2188.506>.
- [39] K. S. Virbhadra and G. F. R. Ellis, “Schwarzschild black hole lensing,” *Phys. Rev. D* **62** (Sep, 2000) 084003, <https://link.aps.org/doi/10.1103/PhysRevD.62.084003>.
- [40] V. Perlick, “Gravitational Lensing from a Spacetime Perspective,” [arXiv:1010.3416](https://arxiv.org/abs/1010.3416) [gr-qc].
- [41] P. V. P. Cunha and C. A. R. Herdeiro, “Shadows and strong gravitational lensing: a brief review,” *Gen. Rel. Grav.* **50** no. 4, (2018) 42, [arXiv:1801.00860](https://arxiv.org/abs/1801.00860) [gr-qc].
- [42] T. Bronzwaer and H. Falcke, “The Nature of Black Hole Shadows,” *Astrophys. J.* **920** no. 2, (2021) 155, [arXiv:2108.03966](https://arxiv.org/abs/2108.03966) [astro-ph.HE].
- [43] V. Perlick and O. Y. Tsupko, “Calculating black hole shadows: Review of analytical studies,” *Phys. Rept.* **947** (2022) 1–39, [arXiv:2105.07101](https://arxiv.org/abs/2105.07101) [gr-qc].
- [44] R. Kumar and S. G. Ghosh, “Black Hole Parameter Estimation from Its Shadow,” *Astrophys. J.* **892** (2020) 78, [arXiv:1811.01260](https://arxiv.org/abs/1811.01260) [gr-qc].
- [45] S. G. Ghosh, R. Kumar, and S. U. Islam, “Parameters estimation and strong gravitational lensing of nonsingular Kerr-Sen black holes,” *JCAP* **03** (2021) 056, [arXiv:2011.08023](https://arxiv.org/abs/2011.08023) [gr-qc].
- [46] M. Afrin, R. Kumar, and S. G. Ghosh, “Parameter estimation of hairy Kerr black holes from its shadow and constraints from M87*,” *Mon. Not. Roy. Astron. Soc.* **504** (2021) 5927–5940, [arXiv:2103.11417](https://arxiv.org/abs/2103.11417) [gr-qc].
- [47] S. G. Ghosh and M. Afrin, “Constraining Kerr-like black holes with Event Horizon Telescope results of Sgr A*,” [arXiv:2206.02488](https://arxiv.org/abs/2206.02488) [gr-qc].
- [48] Z. Younsi, D. Psaltis, and F. Özel, “Black Hole Images as Tests of General Relativity: Effects of Spacetime Geometry,” [arXiv:2111.01752](https://arxiv.org/abs/2111.01752) [astro-ph.HE].

- [49] D. Psaltis, “Testing General Relativity with the Event Horizon Telescope,” *Gen. Rel. Grav.* **51** no. 10, (2019) 137, [arXiv:1806.09740 \[astro-ph.HE\]](#).
- [50] Y. Mizuno, Z. Younsi, C. M. Fromm, O. Porth, M. De Laurentis, H. Olivares, H. Falcke, M. Kramer, and L. Rezzolla, “The Current Ability to Test Theories of Gravity with Black Hole Shadows,” *Nature Astron.* **2** no. 7, (2018) 585–590, [arXiv:1804.05812 \[astro-ph.GA\]](#).
- [51] A. Stepanian, S. Khlghatyan, and V. G. Gurzadyan, “Black hole shadow to probe modified gravity,” *Eur. Phys. J. Plus* **136** no. 1, (2021) 127, [arXiv:2101.08261 \[gr-qc\]](#).
- [52] R. Kumar Walia, S. G. Ghosh, and S. D. Maharaj, “Testing Rotating Regular Metrics with EHT Results of Sgr A*,” *Astrophys. J.* **939** (2022) 77, [arXiv:2207.00078 \[gr-qc\]](#).
- [53] S. Vagnozzi *et al.*, “Horizon-scale tests of gravity theories and fundamental physics from the Event Horizon Telescope image of Sagittarius A*,” [arXiv:2205.07787 \[gr-qc\]](#).
- [54] I. Banerjee, S. Sau, and S. SenGupta, “Signatures of regular black holes from the shadow of Sgr A* and M87*,” *JCAP* **09** (2022) 066, [arXiv:2206.12125 \[gr-qc\]](#).
- [55] I. Banerjee, S. Chakraborty, and S. SenGupta, “Hunting extra dimensions in the shadow of Sgr A*,” *Phys. Rev. D* **106** no. 8, (2022) 084051, [arXiv:2207.09003 \[gr-qc\]](#).
- [56] R. Shaikh, “Black hole shadow in a general rotating spacetime obtained through newman-janis algorithm,” *Phys. Rev. D* **100** (Jul, 2019) 024028. <https://link.aps.org/doi/10.1103/PhysRevD.100.024028>.
- [57] C. Bambi, K. Freese, S. Vagnozzi, and L. Visinelli, “Testing the rotational nature of the supermassive object M87* from the circularity and size of its first image,” *Phys. Rev. D* **100** no. 4, (2019) 044057, [arXiv:1904.12983 \[gr-qc\]](#).
- [58] S. Vagnozzi and L. Visinelli, “Hunting for extra dimensions in the shadow of M87*,” *Phys. Rev. D* **100** no. 2, (2019) 024020, [arXiv:1905.12421 \[gr-qc\]](#).
- [59] A. Allahyari, M. Khodadi, S. Vagnozzi, and D. F. Mota, “Magnetically charged black holes from non-linear electrodynamics and the Event Horizon Telescope,” *JCAP* **02** (2020) 003, [arXiv:1912.08231 \[gr-qc\]](#).
- [60] M. Khodadi, A. Allahyari, S. Vagnozzi, and D. F. Mota, “Black holes with scalar hair in light of the Event Horizon Telescope,” *JCAP* **09** (2020) 026, [arXiv:2005.05992 \[gr-qc\]](#).
- [61] R. Roy, S. Vagnozzi, and L. Visinelli, “Superradiance evolution of black hole shadows revisited,” *Phys. Rev. D* **105** no. 8, (2022) 083002, [arXiv:2112.06932 \[astro-ph.HE\]](#).
- [62] R. Shaikh, K. Pal, K. Pal, and T. Sarkar, “Constraining alternatives to the Kerr black hole,” *Mon. Not. Roy. Astron. Soc.* **506** no. 1, (2021) 1229–1236, [arXiv:2102.04299 \[gr-qc\]](#).
- [63] R. Ghosh, M. Rahman, and A. K. Mishra, “Regularized Stable Kerr Black Hole: Cosmic Censorships, Shadow and Quasi-Normal Modes,” [arXiv:2209.12291 \[gr-qc\]](#).

- [64] R. C. Bernardo and C.-Y. Chen, “Dressed black holes in the new tensor-vector-scalar theory,” [arXiv:2202.08460 \[gr-qc\]](#).
- [65] **Event Horizon Telescope** Collaboration, D. Psaltis *et al.*, “Gravitational Test Beyond the First Post-Newtonian Order with the Shadow of the M87 Black Hole,” *Phys. Rev. Lett.* **125** no. 14, (2020) 141104, [arXiv:2010.01055 \[gr-qc\]](#).
- [66] F. Atamurotov, A. Abdujabbarov, and B. Ahmedov, “Shadow of rotating non-kerr black hole,” *Phys. Rev. D* **88** (Sep, 2013) 064004. <https://link.aps.org/doi/10.1103/PhysRevD.88.064004>.
- [67] F. Atamurotov, A. Abdujabbarov, and B. Ahmedov, “Shadow of rotating Hořava-Lifshitz black hole,” *Astrophys. Space Sci.* **348** (2013) 179–188.
- [68] A. Abdujabbarov, F. Atamurotov, Y. Kucukakca, B. Ahmedov, and U. Camci, “Shadow of Kerr-Taub-NUT black hole,” *Astrophys. Space Sci.* **344** (2013) 429–435, [arXiv:1212.4949 \[physics.gen-ph\]](#).
- [69] F. Atamurotov, K. Jusufi, M. Jamil, A. Abdujabbarov, and M. Azreg-Aïnou, “Axion-plasmon or magnetized plasma effect on an observable shadow and gravitational lensing of a Schwarzschild black hole,” *Phys. Rev. D* **104** no. 6, (2021) 064053, [arXiv:2109.08150 \[gr-qc\]](#).
- [70] U. Papnoi and F. Atamurotov, “Rotating charged black hole in 4D Einstein–Gauss–Bonnet gravity: Photon motion and its shadow,” *Phys. Dark Univ.* **35** (2022) 100916, [arXiv:2111.15523 \[gr-qc\]](#).
- [71] B.-H. Lee, W. Lee, and Y. S. Myung, “Shadow cast by a rotating black hole with anisotropic matter,” *Phys. Rev. D* **103** no. 6, (2021) 064026, [arXiv:2101.04862 \[gr-qc\]](#).
- [72] I. Dymnikova and K. Kraav, “Identification of a regular black hole by its shadow,” *Universe* **5** no. 7, (2019). <https://www.mdpi.com/2218-1997/5/7/163>.
- [73] S. G. Ghosh, M. Amir, and S. D. Maharaj, “Ergosphere and shadow of a rotating regular black hole,” *Nuclear Physics B* **957** (2020) 115088. <https://www.sciencedirect.com/science/article/pii/S0550321320301747>.
- [74] R. Kumar, S. G. Ghosh, and A. Wang, “Shadow cast and deflection of light by charged rotating regular black holes,” *Phys. Rev. D* **100** (Dec, 2019) 124024. <https://link.aps.org/doi/10.1103/PhysRevD.100.124024>.
- [75] A. Abdujabbarov, M. Amir, B. Ahmedov, and S. G. Ghosh, “Shadow of rotating regular black holes,” *Phys. Rev. D* **93** (May, 2016) 104004. <https://link.aps.org/doi/10.1103/PhysRevD.93.104004>.
- [76] N. Tsukamoto, “Black hole shadow in an asymptotically flat, stationary, and axisymmetric spacetime: The kerr-newman and rotating regular black holes,” *Phys. Rev. D* **97** (Mar, 2018) 064021. <https://link.aps.org/doi/10.1103/PhysRevD.97.064021>.

- [77] Z. Li and C. Bambi, “Measuring the kerr spin parameter of regular black holes from their shadow,” *Journal of Cosmology and Astroparticle Physics* **2014** no. 01, (Jan, 2014) 041.
<https://dx.doi.org/10.1088/1475-7516/2014/01/041>.
- [78] I. Banerjee, S. Sau, and S. SenGupta, “Do shadows of Sgr A* and M87* indicate black holes with a magnetic monopole charge?,” [arXiv:2207.06034](https://arxiv.org/abs/2207.06034) [gr-qc].
- [79] Y. Gong, Z. Cao, H. Gao, and B. Zhang, “On neutralization of charged black holes,” *Monthly Notices of the Royal Astronomical Society* **488** no. 2, (07, 2019) 2722–2731,
<https://academic.oup.com/mnras/article-pdf/488/2/2722/29002740/stz1904.pdf>.
<https://doi.org/10.1093/mnras/stz1904>.
- [80] J. W. Moffat, “Black Holes in Modified Gravity (MOG),” *Eur. Phys. J. C* **75** no. 4, (2015) 175,
[arXiv:1412.5424](https://arxiv.org/abs/1412.5424) [gr-qc].
- [81] J. W. Moffat, “Regular Rotating MOG Dark Compact Object,” *Eur. Phys. J. C* **81** no. 2, (2021) 119,
[arXiv:1806.01903](https://arxiv.org/abs/1806.01903) [gr-qc].
- [82] E. Ayon-Beato and A. Garcia, “Regular black hole in general relativity coupled to nonlinear electrodynamics,” *Phys. Rev. Lett.* **80** (1998) 5056–5059, [arXiv:gr-qc/9911046](https://arxiv.org/abs/gr-qc/9911046).
- [83] J. L. Walsh, A. J. Barth, L. C. Ho, and M. Sarzi, “The M87 Black Hole Mass from Gas-dynamical Models of Space Telescope Imaging Spectrograph Observations,” **770** no. 2, (June, 2013) 86,
[arXiv:1304.7273](https://arxiv.org/abs/1304.7273) [astro-ph.CO].
- [84] K. Gebhardt and J. Thomas, “The black hole mass, stellar mass-to-light ratio, and dark halo in m87,” *The Astrophysical Journal* **700** no. 2, (Jul, 2009) 1690.
<https://dx.doi.org/10.1088/0004-637X/700/2/1690>.
- [85] N. J. McConnell, C.-P. Ma, K. Gebhardt, S. A. Wright, J. D. Murphy, T. R. Lauer, J. R. Graham, and D. O. Richstone, “Two ten-billion-solar-mass black holes at the centres of giant elliptical galaxies,” *Nature* **480** no. 7376, (Dec, 2011) 215–218. <https://doi.org/10.1038/nature10636>.
- [86] **Event Horizon Telescope** Collaboration, P. Kocherlakota *et al.*, “Constraints on black-hole charges with the 2017 EHT observations of M87*,” *Phys. Rev. D* **103** no. 10, (2021) 104047,
[arXiv:2105.09343](https://arxiv.org/abs/2105.09343) [gr-qc].
- [87] **EHT Collaboration** Collaboration, P. e. a. Kocherlakota, “Constraints on black-hole charges with the 2017 eht observations of m87*,” *Phys. Rev. D* **103** (May, 2021) 104047.
<https://link.aps.org/doi/10.1103/PhysRevD.103.104047>.
- [88] **Event Horizon Telescope** Collaboration, K. Akiyama *et al.*, “First Sagittarius A* Event Horizon Telescope Results. I. The Shadow of the Supermassive Black Hole in the Center of the Milky Way,” *Astrophys. J. Lett.* **930** no. 2, (2022) L12.
- [89] **Event Horizon Telescope** Collaboration, K. Akiyama *et al.*, “First Sagittarius A* Event Horizon Telescope Results. II. EHT and Multiwavelength Observations, Data Processing, and Calibration,” *Astrophys. J. Lett.* **930** no. 2, (2022) L13.

- [90] **Event Horizon Telescope** Collaboration, K. Akiyama *et al.*, “First Sagittarius A* Event Horizon Telescope Results. III. Imaging of the Galactic Center Supermassive Black Hole,” *Astrophys. J. Lett.* **930** no. 2, (2022) L14.
- [91] **Event Horizon Telescope** Collaboration, K. Akiyama *et al.*, “First Sagittarius A* Event Horizon Telescope Results. IV. Variability, Morphology, and Black Hole Mass,” *Astrophys. J. Lett.* **930** no. 2, (2022) L15.
- [92] **Event Horizon Telescope** Collaboration, K. Akiyama *et al.*, “First Sagittarius A* Event Horizon Telescope Results. V. Testing Astrophysical Models of the Galactic Center Black Hole,” *Astrophys. J. Lett.* **930** no. 2, (2022) L16.
- [93] **Event Horizon Telescope** Collaboration, K. Akiyama *et al.*, “First Sagittarius A* Event Horizon Telescope Results. VI. Testing the Black Hole Metric,” *Astrophys. J. Lett.* **930** no. 2, (2022) L17.
- [94] T. Do *et al.*, “Relativistic redshift of the star S0-2 orbiting the Galactic center supermassive black hole,” *Science* **365** no. 6454, (2019) 664–668, [arXiv:1907.10731](https://arxiv.org/abs/1907.10731) [astro-ph.GA].
- [95] **GRAVITY** Collaboration, R. Abuter *et al.*, “Mass distribution in the Galactic Center based on interferometric astrometry of multiple stellar orbits,” *Astron. Astrophys.* **657** (2022) L12, [arXiv:2112.07478](https://arxiv.org/abs/2112.07478) [astro-ph.GA].
- [96] **GRAVITY** Collaboration, R. Abuter *et al.*, “Detection of the Schwarzschild precession in the orbit of the star S2 near the Galactic centre massive black hole,” *Astron. Astrophys.* **636** (2020) L5, [arXiv:2004.07187](https://arxiv.org/abs/2004.07187) [astro-ph.GA].
- [97] A. Abdujabbarov, M. Amir, B. Ahmedov, and S. G. Ghosh, “Shadow of rotating regular black holes,” *Phys. Rev. D* **93** no. 10, (2016) 104004, [arXiv:1604.03809](https://arxiv.org/abs/1604.03809) [gr-qc].
- [98] K. Hioki and K.-i. Maeda, “Measurement of the Kerr Spin Parameter by Observation of a Compact Object’s Shadow,” *Phys. Rev. D* **80** (2009) 024042, [arXiv:0904.3575](https://arxiv.org/abs/0904.3575) [astro-ph.HE].
- [99] T.-C. Ma, H.-X. Zhang, P.-Z. He, H.-R. Zhang, Y. Chen, and J.-B. Deng, “Shadow cast by a rotating and nonlinear magnetic-charged black hole in perfect fluid dark matter,” *Mod. Phys. Lett. A* **36** no. 17, (2021) 2150112, [arXiv:2010.00151](https://arxiv.org/abs/2010.00151) [gr-qc].
- [100] L. Modesto, J. W. Moffat, and P. Nicolini, “Black holes in an ultraviolet complete quantum gravity,” *Phys. Lett. B* **695** (2011) 397–400, [arXiv:1010.0680](https://arxiv.org/abs/1010.0680) [gr-qc].
- [101] A. Eichhorn, A. Held, and P.-V. Johannsen, “Universal signatures of singularity-resolving physics in photon rings of black holes and horizonless objects,” *Journal of Cosmology and Astroparticle Physics* **2023** no. 01, (Jan, 2023) 043. <https://dx.doi.org/10.1088/1475-7516/2023/01/043>.